Entanglements in a coupled cavity–array with one oscillating end-mirror*

Wu Qin(吴 琴)[a)b)], Xiao Yin(肖 银)[a)], and Zhang Zhi-Ming(张智明)[a)†]

[a)] *Guangdong Provincial Key Laboratory of Nanophotonic Functional Materials and Devices (SIPSE), Guangdong Provincial Key Laboratory of Quantum Engineering and Quantum Materials, South China Normal University, Guangzhou* 510006, *China*

[b)] *School of Information Engineering, Guangdong Medical University, Dongguan* 523808, *China*

(Received 6 March 2015; revised manuscript received 21 April 2015; published online 20 August 2015)

We theoretically investigate the entanglement properties in a hybrid system consisting of an optical cavity–array coupled to a mechanical resonator. We show that the steady state of the system presents bipartite continuous variable entanglement in an experimentally accessible parameter regime. The effects of the cavity–cavity coupling strength on the bipartite entanglements in the field–mirror subsystem and in the field–field subsystem are studied. We further find that the entanglement between the adjacent cavity and the movable mirror can be entirely transferred to the distant cavity and mirror by properly choosing the cavity detunings and the coupling strength in the two-cavity case. Surprisingly, such a remote macroscopic entanglement tends to be stable in the large coupling regime and persists for environment temperatures at above 25 K in the three-cavity case. Such optomechanical systems can be used for the realization of continuous variable quantum information interfaces and networks.

Keywords: entanglement, coupled-cavity array, optomechanical system

PACS: 42.50.Wk, 46.80.+j, 41.20.Cv **DOI:** 10.1088/1674-1056/24/10/104208

1. Introduction

Entanglement, an important trait in quantum mechanics, has become a key resource for many quantum processes.[1] Entanglement can be experimentally prepared and manipulated in microscopic systems, such as photons, ions, and atoms.[2] However, it is not yet completely clear to what extent quantum mechanics applies to macroscopic objects. Quantum phenomena such as entanglement generally do not appear in the macroscopic world due to environment-induced decoherence, which is thought to be the main cause that reduces any quantum superposition to a classical statistical mixture.[3] Nonetheless, with the spectacular level of experimental advancements, it has been possible to see macroscopic quantum superpositions.[4]

Cavity optomechanical systems have become important candidates for exploring what extent of quantum entanglement we can obtain at the macroscopic level[5–13] due to the rapid progress of nanotechnology. The simplest scheme capable of generating stationary optomechanical entanglement is studied in a typical optomechanical setup,[14] where the entanglement between the cavity and the movable mirror is remarkable for its simplicity and robustness against temperature. In recent years, various schemes to generate bipartite entanglements have been proposed, such as the field–mirror entanglement,[15–20] and the mirror–mirror entanglement.[21–24] These studies show that entanglement can be influenced by the factors of the cavity optomechanical system such as the intensity of incident laser and the cavity–pump field detuning. In fact, entangled optomechanical systems have potential profitable applications in realizing quantum communication networks, in which the mechanical modes play the vital role of local nodes where quantum information can be stored and retrieved, and optical modes carry the information between the nodes. This allows the implementation of continuous variable (CV) quantum teleportation,[25,26] quantum telecloning,[27] and entanglement swapping.[28]

Recently, much attention has been focused on the coupled cavity–array (CCA),[29,30] for which some potential technologies have been demonstrated in experiment.[31,32] The system is thought to be suitable for building a large-scale architecture for quantum information processing.[33] These observations remind us of the necessity to explore the entanglement properties in a CCA with one oscillating end-mirror. Different from the conventional CCA with a fixed end-mirror, the end mirror in our system is modelled as a quantum-mechanical harmonic oscillator. Due to the long decoherence of the mechanical harmonic oscillator, the information storage time of the mechanical harmonic oscillator is longer than the field. Hence, it is helpful to the study of information transfer and information

*Project supported by the Major Research Plan of the National Natural Science Foundation of China (Grant No. 91121023), the National Natural Science Foundation of China (Grant Nos. 61378012 and 60978009), the Specialized Research Fund for the Doctoral Program of Higher Education of China (Grant No. 20124407110009), the National Basic Research Program of China (Grant Nos. 2011CBA00200 and 2013CB921804), and the Program for Changjiang Scholar and Innovative Research Team in Universities, China (Grant No. IRT1243).

†Corresponding author. E-mail: zmzhang@scnu.edu.cn

© 2015 Chinese Physical Society and IOP Publishing Ltd

storage in the quantum information processing. In this paper, we investigate the stationary bipartite CV entanglement in this coupled system quantified by the logarithmic negativity. We also show how the stationary entanglement between the adjacent optical cavity field and the mirror can be transferred to the remote optical cavity field and the mirror by selecting appropriately the cavity–pump field detunings and the coupling strength between coupled cavities. However, the field–field entanglement is small at the same time. Moreover, such distant entanglement between two non-interacting subsystems is robust against temperature above 25 K.

The remainder of this paper is organized as follows. In Section 2 we present the model under study and the analytical expressions of the optomechanical system, derive the quantum Langevin equations and the steady state of the system. In Section 3, we quantify the entanglement properties of the system by using the logarithmic negativity. Finally we draw our conclusions in Section 4.

2. Model and equations of motion

As schematically shown in Fig. 1, the system consists of n coupled cavities $(1,2,3,\ldots,N)$ with coupling constant J. Cavity 1 is driven by a pump field, and cavity N consists of an oscillating mirror at one end, modelled as a quantum-mechanical harmonic oscillator. In the rotating frame with frequency ω_0 of the pump field, the Hamilton is given by

$$\begin{aligned} H &= \sum_{j=1}^{N}\hbar\Delta_j a_j^{\dagger}a_j+\sum_{j=1}^{N-1}\hbar J(a_j^{\dagger}a_{j+1}+a_{j+1}^{\dagger}a_j)\\ &\quad+\frac{\hbar\omega_m}{2}(p^2+q^2)-\hbar g a_N^{\dagger}a_N q+\mathrm{i}\hbar E(a_1^{\dagger}-a_1), \end{aligned} \quad (1)$$

where a_j $(a_j^{\dagger})$ is the annihilation (creation) operator for the j-th cavity mode, and $\Delta_j=\omega_j-\omega_0$ is the detuning of its frequencies from the pump laser, which couples to cavity 1 with amplitude E. E is related to the input power P and the cavity damping rate κ by $|E|=\sqrt{2P\kappa/\hbar\omega_0}$. $g=(\omega_0/L)\sqrt{\hbar/m\omega_m}$ denotes the coupling between the mirror and cavity N, the operator q (p) is the dimensionless position (momentum) of the mechanical oscillator with frequency ω_m.

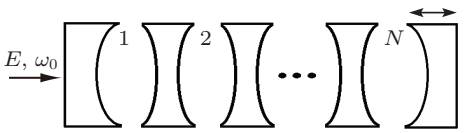


Fig. 1. The model: A coupled cavity–array with one oscillating end-mirror.

Using the Heisenberg equations of motion, and taking into account the corresponding damping and noise terms, we can get the quantum Langevin equations for the operators of the mechanical and optical modes

$$\begin{aligned} \dot{q} &= \omega_m p,\\ \dot{p} &= -\omega_m q+g a_N^{\dagger}a_N-\gamma_m p+\xi,\\ \dot{a}_1 &= -\mathrm{i}\Delta_1 a_1-\mathrm{i}Ja_2+E-\kappa a_1+\sqrt{2\kappa}a_1^{\mathrm{in}},\\ &\vdots\\ \dot{a}_j &= -\mathrm{i}\Delta_j a_j-\mathrm{i}Ja_{j-1}-\mathrm{i}Ja_{j+1}-\kappa a_j+\sqrt{2\kappa}a_j^{\mathrm{in}},\\ &\vdots\\ \dot{a}_N &= -\mathrm{i}\Delta_N a_N-\mathrm{i}Ja_{N-1}+\mathrm{i}g a_N q-\kappa a_N+\sqrt{2\kappa}a_N^{\mathrm{in}}, \end{aligned} \quad (2)$$

in which we have assumed that all cavity–fields have the same decay rate κ. The mechanical oscillator is connected to a thermal bath at a damping rate γ_m with a mean thermal excitation number $\bar{n}=1/(\mathrm{e}^{\hbar\omega_m/k_{\mathrm{B}}T}-1)$, where k_{B} is the Boltzmann constant and T is the temperature of the mechanical bath. The mechanical mode is also affected by a random Brownian force ξ with correlation function $\langle\xi(t)\xi(t')\rangle\simeq\gamma_m(2\bar{n}+1)\delta(t-t')$. Furthermore, a_j^{in} represents the input vacuum noise operator and its nonzero correlation function is $\langle a_j^{\mathrm{in}}(t)a_j^{\dagger\mathrm{in}}(t')\rangle=\delta(t-t')$. In the following, we will focus on the case of two coupled cavities $(N=2)$ and the case of three coupled cavities $(N=3)$.

2.1. The case of two coupled cavities

The steady-state mean values of the system can be obtained by setting the time derivatives to zero:

$$\begin{aligned} p_{\mathrm{s}} &= 0,\\ q_{\mathrm{s}} &= \frac{g|a_{2\mathrm{s}}|^2}{\omega_m},\\ a_{2\mathrm{s}} &= \frac{-\mathrm{i}Ja_{1\mathrm{s}}}{\kappa+\mathrm{i}\Delta_2'},\\ a_{1\mathrm{s}} &= \frac{E}{\kappa+\mathrm{i}\Delta_1+J^2/(\kappa+\mathrm{i}\Delta_2')}, \end{aligned} \quad (3)$$

where $\Delta_2'=\Delta_2-gq_{\mathrm{s}}$ is the effective cavity detuning.

We can divide each Heisenberg operator as a steady-state value plus an additional fluctuation operator with zero-mean value, i.e., $q=q_{\mathrm{s}}+\delta q, p=p_{\mathrm{s}}+\delta p, a_j=a_{j\mathrm{s}}+\delta a_j$ $(j=1,2)$, and get the linearized Langevin equations by neglecting some small quantities

$$\begin{aligned} \delta\dot{q} &= \omega_m\delta p,\\ \delta\dot{p} &= -\omega_m\delta q+G_1(\delta a_2+\delta a_2^{\dagger})-\gamma_m\delta p+\xi,\\ \delta\dot{a}_1 &= -(\kappa+\mathrm{i}\Delta_1)\delta a_1-\mathrm{i}J\delta a_2+\sqrt{2\kappa}a_1^{\mathrm{in}},\\ \delta\dot{a}_2 &= -(\kappa+\mathrm{i}\Delta_2')\delta a_2-\mathrm{i}J\delta a_1+\mathrm{i}G_1\delta q+\sqrt{2\kappa}a_2^{\mathrm{in}}, \end{aligned} \quad (4)$$

where $G_1=ga_{2\mathrm{s}}$ is the effective coupling strength.

2.2. The case of three coupled cavities

In a similar way, we can get the steady-state mean values in the case of three cavities

$$p_{\mathrm{s}} = 0,$$

$$
\begin{aligned}
q_{\rm s} &= \frac{g|a_{3\rm s}|^2}{\omega_m},\\
a_{3\rm s} &= \frac{-{\rm i}Ja_{2\rm s}}{\kappa+{\rm i}\Delta_3'},\\
a_{2\rm s} &= \frac{-{\rm i}Ja_{1\rm s}}{\kappa+{\rm i}\Delta_2+J^2/(\kappa+{\rm i}\Delta_3')},\\
a_{1\rm s} &= \frac{E}{\kappa+{\rm i}\Delta_1+J^2/[\kappa+{\rm i}\Delta_2+J^2/(\kappa+{\rm i}\Delta_3')]},
\end{aligned}
\tag{5}
$$

and the linearized Langevin equations

$$
\begin{aligned}
\delta\dot{q} &= \omega_m\delta p,\\
\delta\dot{p} &= -\omega_m\delta q+G_2(\delta a_3+\delta a_3^\dagger)-\gamma_m\delta p+\xi,\\
\delta\dot{a}_1 &= -{\rm i}\Delta_1\delta a_1-{\rm i}J\delta a_2-\kappa\delta a_1+\sqrt{2\kappa}a_{1\rm in},\\
\delta\dot{a}_2 &= -{\rm i}\Delta_2\delta a_2-{\rm i}J\delta a_1-{\rm i}J\delta a_3-\kappa\delta a_2+\sqrt{2\kappa}a_{2\rm in},\\
\delta\dot{a}_3 &= -{\rm i}\Delta_3'\delta a_3-{\rm i}J\delta a_2+{\rm i}G_2\delta q-\kappa\delta a_3+\sqrt{2\kappa}a_{3\rm in},
\end{aligned}
\tag{6}
$$

where $\Delta_3'=\Delta_3-gq_{\rm s}$, $G_2=ga_{3\rm s}$.

3. Entanglement

In this section we mainly study the entanglement between any two subsystems in this system. Here we define the cavity field quadratures

$$
\begin{aligned}
\delta X_j &= (\delta a_j+\delta a_j^\dagger)/\sqrt{2},\\
\delta Y_j &= (\delta a_j-\delta a_j^\dagger)/{\rm i}\sqrt{2},
\end{aligned}
\tag{7}
$$

and the corresponding Hermitian input noise operators

$$
\begin{aligned}
X_j^{\rm in} &= (a_j^{\rm in}+a_j^{\dagger{\rm in}})/\sqrt{2},\\
Y_j^{\rm in} &= (a_j^{\rm in}-a_j^{\dagger{\rm in}})/{\rm i}\sqrt{2}.
\end{aligned}
\tag{8}
$$

Then equations (4) and (6) can be rewritten as a matrix form

$$
\dot{u}(t)=Au(t)+n(t),
\tag{9}
$$

in which the transposes of the column vector $u(t)$, $n(t)$ can be expressed as

$$
\begin{aligned}
u^{\rm T}(t) &= (\delta q(t),\delta p(t),\delta X_1(t),\delta Y_1(t),\delta X_2(t),\delta Y_2(t)),\\
n^{\rm T}(t) &= (0,\xi(t),\sqrt{2\kappa}X_1^{\rm in}(t),\sqrt{2\kappa}Y_1^{\rm in}(t),\\
&\quad \sqrt{2\kappa}X_2^{\rm in}(t),\sqrt{2\kappa}Y_2^{\rm in}(t)),
\end{aligned}
\tag{10}
$$

in the case of two coupled cavities, and

$$
\begin{aligned}
u^{\rm T}(t) &= (\delta q(t),\delta p(t),\delta X_1(t),\delta Y_1(t),\delta X_2(t),\\
&\quad \delta Y_2(t),\delta X_3(t),\delta Y_3(t)),\\
n^{\rm T}(t) &= (0,\xi(t),\sqrt{2\kappa}X_1^{\rm in}(t),\sqrt{2\kappa}Y_1^{\rm in}(t),\sqrt{2\kappa}X_2^{\rm in}(t),\\
&\quad \sqrt{2\kappa}Y_2^{\rm in}(t),\sqrt{2\kappa}X_3^{\rm in}(t),\sqrt{2\kappa}Y_3^{\rm in}(t)),
\end{aligned}
\tag{11}
$$

in the case of three coupled cavities. The matrix A in these two cases can be given by

$$
A=\begin{pmatrix}
0 & \omega_m & 0 & 0 & 0 & 0\\
-\omega_m & -\gamma_m & 0 & 0 & G_{2m} & 0\\
0 & 0 & -\kappa & \Delta_1 & 0 & J\\
0 & 0 & -\Delta_1 & -\kappa & -J & 0\\
0 & 0 & 0 & J & -\kappa & \Delta_2'\\
G_{2m} & 0 & -J & 0 & -\Delta_2' & -\kappa
\end{pmatrix}
\tag{12}
$$

and

$$
A=\begin{pmatrix}
0 & \omega_m & 0 & 0 & 0 & 0 & 0 & 0\\
-\omega_m & -\gamma_m & 0 & 0 & 0 & 0 & G_{3m} & 0\\
0 & 0 & -\kappa & \Delta_1 & 0 & J & 0 & 0\\
0 & 0 & -\Delta_1 & -\kappa & -J & 0 & 0 & 0\\
0 & 0 & 0 & J & -\kappa & \Delta_2 & 0 & J\\
0 & 0 & -J & 0 & -\Delta_2 & -\kappa & -J & 0\\
0 & 0 & 0 & 0 & 0 & J & -\kappa & \Delta_3'\\
G_{3m} & 0 & 0 & 0 & -J & 0 & -\Delta_3' & -\kappa
\end{pmatrix}
\tag{13}
$$

respectively, where $G_{2m}=\sqrt{2}G_2$, $G_{3m}=\sqrt{2}G_3$. The solution of Eq. (9) can be expressed as

$$
u(t)=M(t)u(0)+\int_0^t {\rm d}t'M(t')n(t-t'),
\tag{14}
$$

where $M(t)=\exp(At)$. The system is stable only if the real parts of all the eigenvalues of matrix A are negative, which can be derived by applying the Routh–Hurwitz criterion.[34] We will choose the parameters so that the system is subsequently in a steady state. We define $V_{ij}=\langle u_i(\infty)u_j(\infty)+u_j(\infty)u_i(\infty)\rangle/2$, which is a 6×6 (8×8) correlation matrix (CM). Here

$$
u^{\rm T}(\infty)=(\delta q(\infty),\delta p(\infty),\delta X_1(\infty),\delta Y_1(\infty),\delta X_2(\infty),\delta Y_2(\infty))
$$

or

$$
\begin{aligned}
u^{\rm T}(\infty) &= (\delta q(\infty),\delta p(\infty),\delta X_1(\infty),\delta Y_1(\infty),\\
&\quad \delta X_2(\infty),\delta Y_2(\infty),\delta X_3(\infty),\delta Y_3(\infty))
\end{aligned}
$$

is the vector of continuous variables fluctuations operators at the steady state. When the system is stable ($t\to\infty$), we get

$$
V_{ij}=\sum_{k,l}\int_0^\infty {\rm d}t\int_0^\infty {\rm d}t'M_{ik}(t)M_{jl}(t')\Phi_{kl}(t-t'),
\tag{15}
$$

where $\Phi_{kl}(t-t')=(\langle n_k(t)n_l(t')+n_l(t')n_k(t)\rangle)/2$ is the steady-state noise CM. When the stability conditions are satisfied, the steady-state CM satisfies a Lyapunov equation

$$
AV+VA^{\rm T}=-D,
\tag{16}
$$

where $D=\mathrm{diag}[0,\gamma_m(2\bar{n}+1),\kappa,\kappa,\kappa,\kappa]$ ($N=2$) (or $D=\mathrm{diag}[0,\gamma_m(2\bar{n}+1),\kappa,\kappa,\kappa,\kappa,\kappa,\kappa]$ ($N=3$)). We can straightforwardly have the solution of the CM with Eq. (16). However, the explicit expression is too complicated and will not be reported here.

Then we will examine the entanglement properties of the steady state of the tripartite system under consideration. For

this purpose, we consider the entanglement of the possible bipartite subsystems that can be obtained by tracing over the remaining degrees of the freedom. This bipartite entanglement will be quantified by using the logarithmic negativity

$$E_N = \max[0, -\ln 2\eta^-], \tag{17}$$

where

$$\eta^- \equiv 2^{-1/2}\left[\sum(V_{\rm bp}) - \sqrt{\Sigma(V_{\rm bp})^2 - 4\det(V_{\rm bp})}\right]^{1/2}$$

is the lowest symplectic eigenvalue of the partial transpose of the 4×4 CM, $V_{\rm bp}$, associated with the selected bipartition, obtained by neglecting the rows and columns of the uninteresting mode,

$$V_{\rm bp} = \begin{pmatrix} B & C \\ C_T & B' \end{pmatrix}, \tag{18}$$

and $\Sigma(V_{\rm bp}) \equiv \det B + \det B' - 2\det C$.

3.1. Numerical calculation for two-cavity case

Firstly, we will study the optomechanical entanglement in two coupled cavities case. In order to investigate the behavior of CV entanglement between the elements of the tripartite system in this case, we will denote the logarithmic negativity for the mirror–cavity 1, mirror–cavity 2, and cavity 1–cavity 2 entanglements as E_N^1, E_N^2, and E_N^3, respectively. In our numerical calculations, we will use the set of parameters for the optomechanical system given in Table 1, which match the current experimental state, thus making our proposal very close to feasibility.

Table 1. The parameters used in our numerical calculations, taken from the experiments in Ref. [35].

Paramter	Symbol	Value
Mechanical mass	m	5 ng
Mechanical frequency	$\omega_m/2\pi$	100 Hz
Mechanical damping rate	$\gamma_m/2\pi$	100 Hz
Cavity length	L	1 mm
Input power	P	50 mW
Cavity–field wavelength	λ	810 nm
Optical damping rate	κ	34.1 MHz

For the sake of simplicity, we assume $-\Delta_1 = \Delta_2' = \Delta$. In Fig. 2, we have plotted the three bipartite logarithmic negativities E_N^1 (dashed curves), E_N^2 (solid curves), and E_N^3 (dash–dotted curves), versus the normalized detuning Δ/ω_m at a fixed temperature of $T = 400$ mK for four values of the coupling strength $J = 0.4\omega_m$ (Fig. 2(a)), $J = 0.6\omega_m$ (Fig. 2(b)), $J = 0.8\omega_m$ (Fig. 2(c)), and $J = \omega_m$ (Fig. 2(d)). It can be clearly seen that the bipartite entanglement E_N^1 is enhanced while the bipartite entanglement E_N^2 is decreased and the bipartite entanglement E_N^3 is almost unchanged with the increase of J. That is to say, the entanglement between mirror and cavity 1 (remote cavity) increases at the expense of mirror and cavity 2 (adjacent cavity) entanglement, and the adjacent cavity serves as an entanglement transmitter in this process. More importantly, under the increasing action of cavity–cavity coupling, the range of the entanglement between two distant subsystems (mirror and cavity 1) can be broader, i.e., from $\Delta/\omega_m \in [0.5, 1.5]$ in Fig. 2(a) to $\Delta/\omega_m \in [0.3, 2]$ in Fig. 2(d). The more broader effective detuning is obtained, the more easily it is realized in experiment.

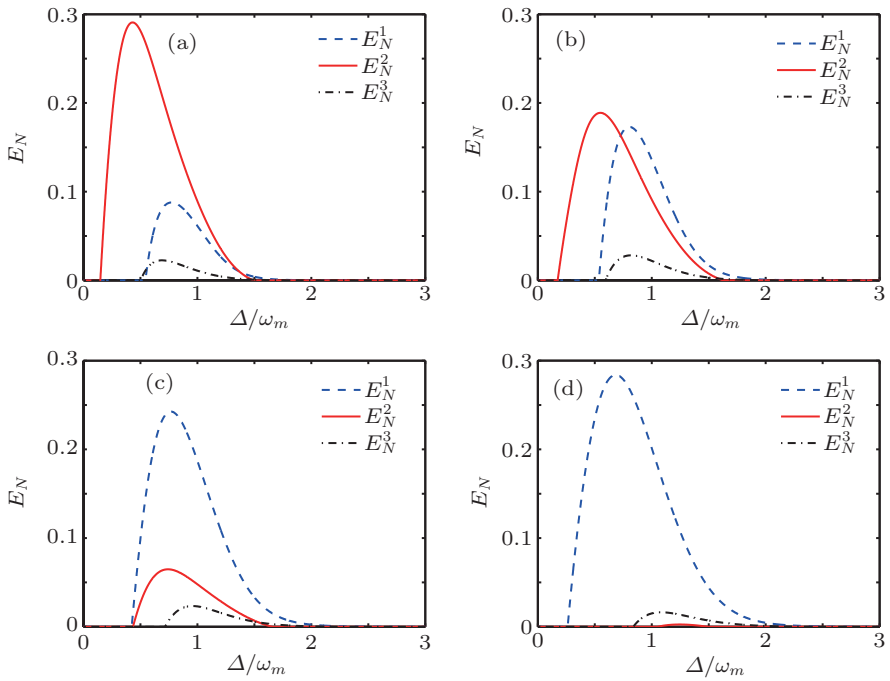


Fig. 2. (color online) Plot of the logarithmic negativity E_N^1 (dashed curves), E_N^2 (solid curves) and E_N^3 (dash–dotted curves) as a function of the normalized detuning Δ/ω_m at a fixed temperature $T = 400$ mK. (a) $J = 0.4\omega_m$, (b) $J = 0.6\omega_m$, (c) $J = 0.8\omega_m$, (d) $J = \omega_m$.

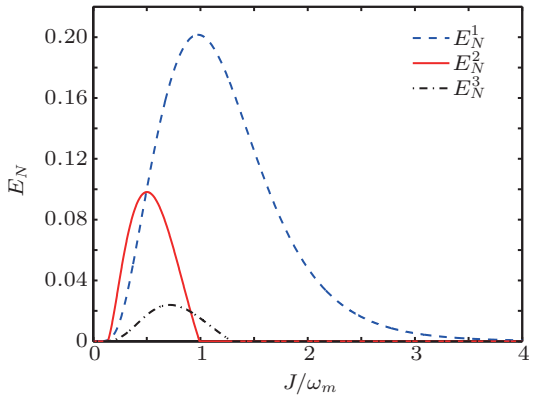


Fig. 3. (color online) Plot of the logarithmic negativity E_N^1 (dashed curves), E_N^2 (solid curves), and E_N^3 (dash–dotted curves) versus the coupling strength J when $\Delta_1 = -\omega_m, \Delta_2 = \omega_m$.

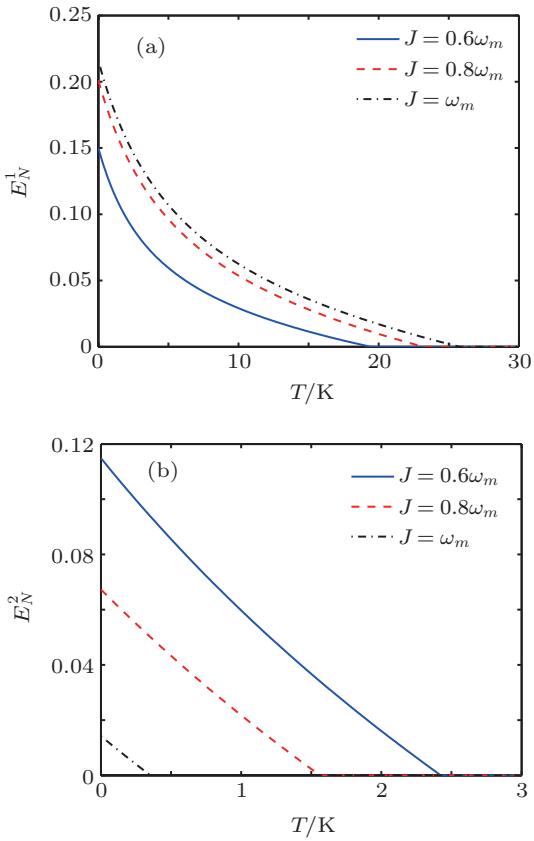


Fig. 4. (color online) Plot of the logarithmic negativities E_N^1 (a) and E_N^2 (b) versus the environment temperature when $\Delta_1 = -\omega_m$, $\Delta_2 = \omega_m$. The solid, dashed, and dash–dotted lines are corresponding to different coupling strengths $J = 0.6\omega_m$, $0.8\omega_m$, and ω_m, respectively.

For clearly presenting the effect of cavity–cavity coupling strength on the optomechanical entanglement, we plot E_N^1, E_N^2, and E_N^3 with respect to J in Fig. 3 where cavity 1 is driven on the blue sideband, $\Delta_1 = -\omega_m$, and cavity 2 on the red sideband, $\Delta_2 = \omega_m$. This figure shows that the three bipartite entanglements increase first and go through a peak at about $J = \omega_m$ (dashed line), $J = 0.5\omega_m$ (solid line), $J = 0.75\omega_m$ (dash–dotted line), then drop close to zero. It is worth noting that the optimal entanglement between mirror and cavity 1 is reached at $J = \omega_m$ when the entanglement between mirror and cavity 2 disappears completely at this point. In our scheme there is no direct interaction between the cavity 1 and mirror, so one may say that the entanglement is entirely transferred from the adjacent cavity to the distant cavity due to the cavity–cavity coupling. Hence, the optomechanical entanglement between the mechanical mode and the optical mode is very sensitive to the coupling strength J. This result reveals that by changing the value of J, one can control the entanglement distribution in the tripartite system, which implies that we can transfer the entanglement to two indirectly coupled subsystems through the coupling of two cavities.

It is also important to understand the behavior of entanglement with respect to the temperature T. We finally discuss the robustness of optomechanical entanglement (E_N^1 and E_N^2) with respect to the environmental temperature, which is shown in Fig. 4. We can see that the optomechanical entanglement between mirror and cavity 1 persists for temperatures above 19 K, as illustrated in Fig. 4(a). Moreover, the logarithmic negativity E_N^1 and its critical value of temperature T_c increase with the increase of J (T_c is defined as $T > T_c, E_N = 0$). However the entanglement of mirror–field 2 is fragile to the environment temperature which disappears at about 2 K. In addition, the stronger the coupling strength, the smaller the logarithmic negativity E_N^1, and the lower the critical value of temperature T_c, as seen in Fig. 4(b).

3.2. Numerical calculation for three-cavity case

Then we will investigate the optomechanical entanglement properties in the case of three coupled cavities. In this case, we mainly discuss the entanglement between the three cavities and mirror since the entanglement between three cavities is too small. We will denote the logarithmic negativities for the mirror–field 1, mirror–field 2, and mirror–field 3 bimodal partitions as E_N^1, E_N^2, E_N^3, respectively. In the following numerical calculations, the system parameters are taken as the same as the case of two coupled cavities. We also assume $\Delta_1 = -\Delta_2 = \Delta_3' = \Delta$ for simplicity. The three bipartite logarithmic negativities E_N^1 (dashed curves), E_N^2 (solid curves), and E_N^3 (dash–dotted curves) versus the normalized detuning Δ/ω_m are shown in Fig. 5. It is clearly seen that the optimal entanglement is reached at about $\Delta/\omega_m = 0.5$. Moreover, the largest entanglement is the one between the mirror and cavity 2 when $J = \omega_m$, which are indirectly coupled, as seen in Fig. 5(a). With the increasing of coupling strength, the logarithmic negativity E_N^2 decreases, while the logarithmic negativities E_N^1 and E_N^3 increase. We also observed in Fig. 5(d) that the degree of entanglement for mirror–cavity 1 has a similar curve to that of mirror–cavity 3 for a large coupling strength. When $J = 5\omega_m$, the entanglement between mirror and cavity 1 (3) reaches its maximum 0.15 at about $\Delta = 0.5\omega_m$. At the same time, the entanglement between mirror and cavity 2 decreases to 0.02. This indicates that the entanglement is transferred from the middle cavity 2 to cavities (1 and 3) on both sides of cavity 2 with the increase of the coupling strength.

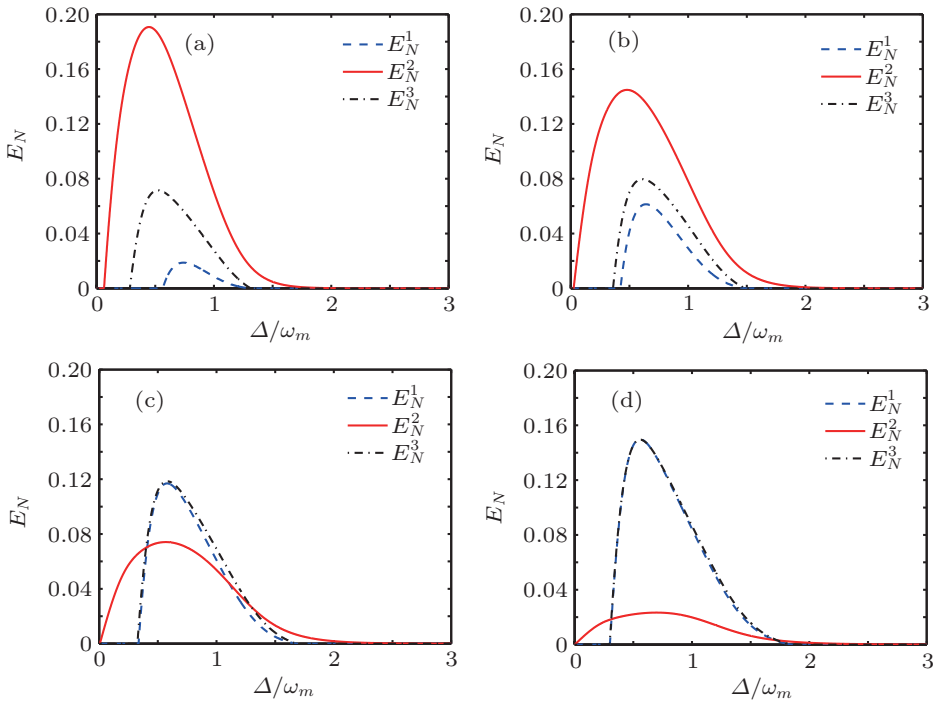


Fig. 5. (color online) Plot of the logarithmic negativity E_N^1 (dashed curves), E_N^2 (solid curves), and E_N^3 (dash–dotted curves) as a function of the normalized detuning Δ/ω_m. (a) $J=\omega_m$, (b) $J=1.5\omega_m$, (c) $J=2.5\omega_m$, (d) $J=5\omega_m$.

In Fig. 6, we also plot the logarithmic negativity E_N^1, E_N^2, and E_N^3 as a function of the coupling strength J when $\Delta_1=\Delta_3'=0.5\omega_m$, $\Delta_2=-\omega_m$, and $T=400$ mK. It is seen obviously from the figure that the maximum entanglement between the mirror and cavity 2 is obtained near $J/\omega_m=1$, and the logarithmic negativity E_N^2 disappears rapidly with the sufficiently large coupling strength J (solid curve). However, the entanglement between the mirror and cavity 1 (3) is enhanced and becomes more stable with the increase of J, which is quite different from Fig. 4. This implies that we can obtain stationary entanglement between two distant subsystems through adjusting the parameter J.

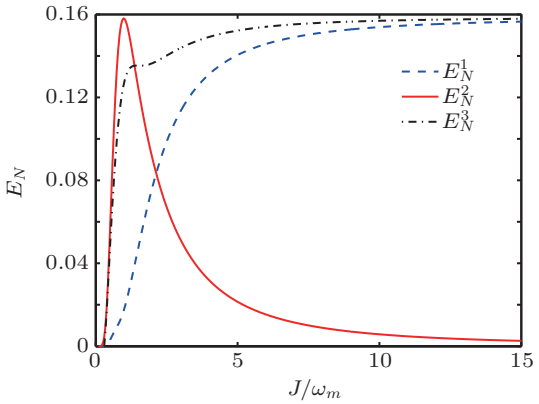


Fig. 6. (color online) Plot of the logarithmic negativity E_N^1 (dashed curve), E_N^2 (solid curve), and E_N^3 (dash–dotted curve) versus the coupling strength J when $\Delta_1=\Delta_3'=0.5\omega_m, \Delta_2=-\omega_m$.

The robustness of the optomechanical entanglement E_N^1, E_N^2 with respect to temperature T is shown in Figs. 7(a) and 7(b), respectively. From this figure, we can see that the entanglement between mirror and cavity 1 rapidly decreases from 0.09 to zero with the environment temperature from 0.1 mK to 3 K when $J=2\omega_m$ (dash–dotted line in Fig. 7(a)).

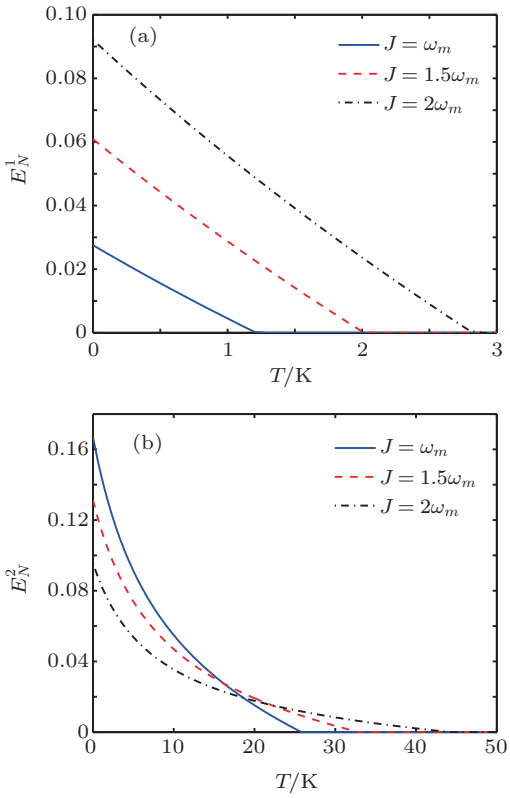


Fig. 7. (color online) Plot of the logarithmic negativity E_N^1 (a) and E_N^2 (b) versus the environment temperature when $\Delta_1=\Delta_3'=0.5\omega_m$, $\Delta_2=-\omega_m$. Solid, dashed, and dash–dotted curves refer to different coupling strengths $J=\omega_m, 1.5\omega_m, 2\omega_m$.

Furthermore, the logarithmic negativity E_N^1 and its critical value of temperature T_c increase with the value of J. It is worth noticing that the entanglement of mirror–cavity 2 becomes more robust to temperature ($T_c = 40$ K, as shown in Fig. 7(b)) although the degree of entanglement decreases with the increasing of J.

4. Conclusion

In conclusion, we have studied the properties of optomechanical entanglement in a coupled cavity–array with a movable mirror through the logarithmic negativity. We mainly considered two cases of a different number of coupled cavity (two and three cavities). Our results show that the entanglement of the adjacent cavity and mirror can be entirely transferred to the remote cavity and mirror due to cavity–cavity coupling in the case of two coupled cavities. Such an optomechanical entanglement between the distant cavity mode and the mechanical mode of the mirror is sensitive to cavity–cavity coupling strength and cavity–pump detunings. The stationary distant entanglement can be achievable through strong cavity–cavity coupling when $\Delta_1 = \Delta_3' = 0.5\omega_m, \Delta_2 = -\omega_m$ in the case of three coupled cavities. It is worth noting that the generated remote entanglement is surprisingly robust against increasing temperature: entanglement may persist above 19 K and 25 K in the two cases. According to our theoretical calculations and analyses, we believe that if we continue to increase the number of cavities, the middle cavities can serve as a signal transmission medium to realize quantum information transfer processing from the nearest cavity to the farthest cavity.

References

[1] Nielson M A and Chuang I L 2000 *Quantum Computation and Quantum Information* (Cambridge: Cambridge University Press)
[2] Horodechi R, Horodecki P, Horodecki M andHorodecki K 2009 *Rev. Mod. Phys.* **81** 865
[3] Zurek W H 2003 *Rev. Mod. Phys.* **75** 715
[4] Friedman J R, Patel V, Chen W, Tolpygo S K and Lukens J E 2000 *Nature* **406** 43
[5] Huang S and Agarwal G S 2011 *Phys. Rev. A* **83** 043826
[6] Brown K R, Ospelkaus C, Colombe Y, *et al.* 2011 *Nature* **471** 196
[7] Liao J Q and Law C K 2011 *Phys. Rev. A* **83** 033820
[8] Ma Y H and Zhou L 2013 *Chin. Phys. B* **22** 024204
[9] Zhang D and Zheng Q 2013 *Chin. Phys. Lett.* **30** 024213
[10] Shi Z S, Xia Y and Song J 2013 *Quantum Inf. Process.* **12** 3179
[11] Dalafi A, Naderi M H, Soltanolkotabi M and Barzanjeh Sh 2013 *J. Phys. B: At. Mol. Opt. Phys.* **46** 235502
[12] Asjad M, Shahzad M A and Saif F 2013 *Eur. Phys. J. D* **67** 198
[13] Sete E A and Eleuch H 2014 *Phys. Rev. A* **89** 013841
[14] Vitali D, Gigan S, Ferreira A, Böhm H R, Tombesi P, Guerreiro A, Vedral V, Zeilinger A and Aspelmeyer M 2007 *Phys. Rev. Lett.* **98** 030405
[15] Genes C, Mari A, Tombesi P and Vitali D 2008 *Phys. Rev. A* **78** 032316
[16] Joshi C, Larson J, Jonson M, Andersson E and Öhberg P 2012 *Phys. Rev. A* **85** 033805
[17] Akram U, Munro W, Nemoto K and Milburn G J 2012 *Phys. Rev. A* **86** 042306
[18] Mi X W, Bai J X and Song K H 2013 *Eur. Phys. J. D* **67** 115
[19] Zhang D, Zhang X P and Zheng Q 2013 *Chin. Phys. B* **22** 064206
[20] Ma Y H and Wu E 2015 *Int. J. Theor. Phys.* **54** 1334
[21] Joshi C, Akram U and Milburn G J 2014 *New. J. Phys.* **16** 023009
[22] Liao J Q, Wu Q Q and Nori F 2014 *Phys. Rev. A* **89** 014302
[23] Ge W C, Al-Amri M, Nha H and Zubairy M S 2013 *Phys. Rev. A* **88** 022338
[24] Huang S and Agarwal G S 2009 *New. J. Phys.* **11** 103044
[25] Mancini S, Vitali D and Tombesi P 2003 *Phys. Rev. Lett.* **90** 137901
[26] Pirandola S, Mancini S, Vitali D and Tombesi P 2003 *Phys. Rev. A* **68** 062317
[27] Pirandola S, Mancini S, Vitali D and Tombesi P 2004 *J. Mod. Opt.* **51** 901
[28] Pirandola S, Vitali D, Tombesi P and Lloyd S 2006 *Phys. Rev. Lett.* **97** 150403
[29] Serafini A, Mancini S and Bose S 2006 *Phys. Rev. Lett.* **96** 010503
[30] Cho J, Angelakis D G and Bose S 2008 *Phys. Rev. A* **78** 022323
[31] Hartmann M J, Brandão F G S L and Plenio M B 2006 *Nat. Phys.* **2** 849
[32] Hartmann M J, Brandão F G S L and Plenio M B 2008 *Laser Photon. Rev.* **2** 527
[33] Yönac M, Yu T and Eberly H J 2006 *J. Phys. B: At. Mol. Opt. Phys.* **39** S621
[34] DeJesus E X and Kaufman C 1987 *Phys. Rev. A* **35** 5288
[35] Kleckner D, Marshall W, Dood M, *et al.* 2006 *Phys. Rev. Lett.* **96** 173901